Development and Experimental Evaluation of Human-Robot Safety of a Series Elastic Joint for Supernumerary Robotic Limbs

XIAO Yao[1], *LIAO Ziyu*[1,2], *QU Wenjie*[1], *CHANG Tianzuo*[1], *LIU Keming*[1], *CHEN Bai*[1*]

1. College of Mechanical and Electrical Engineering, Nanjing University of Aeronautics and Astronautics, Nanjing 210016, P. R. China; 2. Intelligent Manufacturing College, Jinhua University of Vocational Technology, Jinhua 321017, P. R. China

(Received 14 January 2025; revised 29 March 2025; accepted 24 July 2025)

Abstract: Human-robot safety is an important topic in wearable robotics, especially in supernumerary robotic limbs (SRLs). The proposal of flexible joint improves human-robot safety strategy, which allows physical contact between human and robots, rather than strictly limiting the human-robot motion. However, most researchers focus on the variable stiffness features of flexible joints, but few evaluate the performance of the flexible joint in the human-robot collision. Therefore, the performance of two typical flexible joints, including the series elastic joint (SEJ) and the passive variable stiffness joint (PVSJ), are compared through dynamic collision experiments. The results demonstrate that the SEJ absorbs 40.7%—58.7% of the collision force and 34.2%—45.2% of the collision torque in the driven-torque below 4 N·m and driven-speed of 3—7 (°)/s, which is more stable than PVSJ. In addition, the stiffness error of SEJ is measured at 5.1%, significantly lower than the 23.04% measured in the PVSJ. The huge stiffness error of PVSJ leads to its unreliability in buffering collision. Furthermore, we analyze results and confirm that SEJ has a more stable human-robot safety performance in buffering dynamic collision. Consequently, the SEJ is suitable in SRLs for human-robot safety in our scenario.

Key words: supernumerary robotic limbs (SRLs); variable stiffness joint (SEJ); series elastic joint; human-robot safety; wearable robot

CLC number: TP242.6 **Document code:** A **Article ID:** 1005-1120(2025)04-0464-13

0 Introduction

Supernumerary robotic limbs (SRLs)[1-2] are a new type of wearable robot with independently locomotion robotic limbs, and they can be used as the wearer's additional limbs for cooperative operations[3]. Currently, the SRLs face a significant challenge about human-robot safety[4], because the robotic limbs are very close to the human body. And the conventional human-robot safety strategy is no longer suitable for the SRLs. For example, strictly limiting the SRLs' speed[5-6] and range[7-8] of motion will diminish the collaborative efficiency of SRLs greatly and fail to demonstrate the benefits[9]. Allowing some physical contacts between robotic limbs and the human body or biological limbs will have the potential to change human-robot safety strategy of SRLs dramatically. The flexible joint with variable stiffness characteristics offers the possibility of such contact between the wearer and SRLs[10]. Therefore, this paper explores what kind of flexible joints are suitable for safety requires of human-robot collaboration in SRLs.

Flexible joints absorb load impacts via the elastic potential energy of the elastic element between the drive motor and robotic limbs to allow the physical contact between wearer and SRLs[11-12]. When a

*Corresponding author, E-mail address: chenbye@nuaa.edu.cn.

How to cite this article: XIAO Yao, LIAO Ziyu, QU Wenjie, et al. Development and experimental evaluation of human-robot safety of a series elastic joint for supernumerary robotic limbs[J]. Transactions of Nanjing University of Aeronautics and Astronautics, 2025,42(4):464-476.

http://dx.doi.org/10.16356/j.1005-1120.2025.04.003

minor collision occurs, SRLs with flexible joints can become "soft" to ensure human-robot safety without reducing work efficiency. Consequently, this paper believes that the flexible joints in SRLs are very imporcant for the study of human-robot safety, and it is valuable to explore the safety performance of the flexible joints.

The flexible joints can be divided into two categories: Series elastic joints (SEJ)[13] and variable stiffness joints, which are mainly categorized into active variable stiffness joints[14] and passive variable stiffness joints (PVSJ)[15]. PVSJ is widely utilized in wearable robots since it has small size and lighter weight. The SEJ has segmental stiffness properties, which is realized by the deformation of the compression spring. Toubar et al.[16] designed a discrete SEJ based on a unique design topology, it had three adjustable stiffness for using in unstructured environments. However, this SEJ increased the weight of the joint and the complexity of control. The variable stiffness characteristics of PVSJ do not require additional drive units. The stiffness changes with the deflection angle of the mechanism. Qian et al.[17] designed a reconfigurable PVSJ that achieved adjustable stiffness over a wide range from 0.095 N·m/(°) to 2.33 N·m/(°) through a reconfigurable rotational flexible module. In addition, to satisfy the low impedance, the high force control accuracy, and the safe physical human-robot interaction, this flexible module has nonlinear stiffness and multiple stiffness profiles by different configurations.

To evaluate the safety performance of the flexible joints, Chen et al.[18] designed a SEJ with a torsion spring and conducted collision experiments. The collision experiments demonstrated that a low collision energy resulted in a minimal deflection angle of the torsion spring. They evaluated the buffer performance by the deflection angle, but they did not quantitatively measure its buffering capacity. Wang et al.[19] investigated the effect of SEJ on collision forces under different conditions. The result showed that increasing soft covering thickness, decreasing load inertia, collision velocity and joint stiffness could diminish collision force. This provides the basis for the design of flexible joints, but this study did not consider the safety of the robots. Fern'andez et al.[10] designed a SEJ for human-robot safety. But the effectiveness of the human-robot safety was not evaluated, only simulations and experiments were conducted. Wolf et al.[20] proposed a flexible joint for human-robot safety and demonstrated the joint's ability to store energy by experiments. Their works proved indirectly the value of flexible joints in human-robot safety, but they did not quantitatively evaluate the performance of flexible joints. Calanca et al.[21] designed an economical series elastic link by the idea of SEJ and pointed that plastic deformation of the material might also help buffer the impact. Park et al.[22] proposed a PVSJ and conducted dynamic collision experiments to demonstrate its effectiveness in human-robot safety. But this study did not quantitatively measure the buffering capacity or consider the safety of the robots. The above researchers have proposed different approach for achieving human-robot safety in flexible joints, but they did not quantitatively evaluate the buffer performance of the flexible joints. Meanwhile, the safety effectiveness of SRLs with different types of flexible joints needs to be investigated.

In summary, the SEJ and PVSJ are widely used in collaborative wearable robots. However, they exhibit significant differences in human-robot safety performance due to the fundamental differences in variable stiffness actuation principles. This difference may have implications for human-robot safety performance. This paper finds that the PVSJ does not perform stably as well as the SEJ in specific situations. There is no consensus on the effectiveness of SEJ and PVSJ for human-robot safety. Therefore, it will be meaningful to explore the performance differences of two typical flexible joints in human-robot safety and what kind of flexible joint is suitable for SRLs, which can contribute to the realization of safe human-robot interactions for SRLs. This paper designs and manufactures a SEJ with segmental stiffness characteristics. Then explores and analyzes the human-robot safety of SEJ and PVSJ by dynamic collision experiments.

The main contributions of this paper are as follows. (1) A SEJ modular with segmental stiffness characteristics for SRLs is designed and manufactured. (2) The SRLs with SEJ reveal the more stable feature than the PVSJ in dynamic collisions, and the SEJ has better buffering performance than PVSJ in dynamic collisions.

This paper is organized as follows: Section 1 proposes the design indicators of the flexible joints for SRLs based on the requirement of human-robot safety. In Section 2, the SEJ's segmented stiffness model is established and the parameters are optimized. In Section 3, dynamic collision experiments are conducted to compare the SEJ, rigid joint (RJ) and PVSJ, highlighting the human-robot safety effectiveness and the stable performance of the SEJ. Section 4 discusses the hysteresis effect of the PVSJ, analyzes the experiment result, and states the limitation of this work. Finally, Section 5 provides a comprehensive summary of the aforementioned work.

1 Flexible Joint Design Indicators

1.1 Structure of SRLs and operation mode

The SRLs is shown in Fig.1(a), which has 4 degrees of freedom (DOFs) including 2-DOFs in the shoulder, 1-DOF in the elbow, and 1-DOF in the wrist. The elbow joint is actuated by a belt mechanism, elbow motor and two shoulder motors which are both mounted on the base of SRLs to decrease the motion inertia during collaboration.

The connection between flexible joints and SRLs is depicted in Fig.1(b). The flexible joint's input is connected to the shoulder joint motor output flange, and the flexible joint's output flange is connected to the elbow joint motor. This enables the power flexible transmission of the shoulder joint.

This paper designs a collaboration scenario for SRLs to assist in sheet installation. The workflow is shown in Fig.2. It can be seen that the human needs to hold and install the sheet simultaneously, necessitating the SRLs for supporting the sheet. Throughout both the swing and stance periods, the human's biological limb and robotic limbs are in motion, with the shoulder joint constantly providing torque to support the sheet. At the same time, the human-robot workspace partially overlaps, the risk of human-robot collision is significantly elevated. As a result, the shoulder joint of SRLs needs protection especially, and it is necessary to propose a flexible joint for the shoulder to reduce the impact of unexpected human-robot collisions.

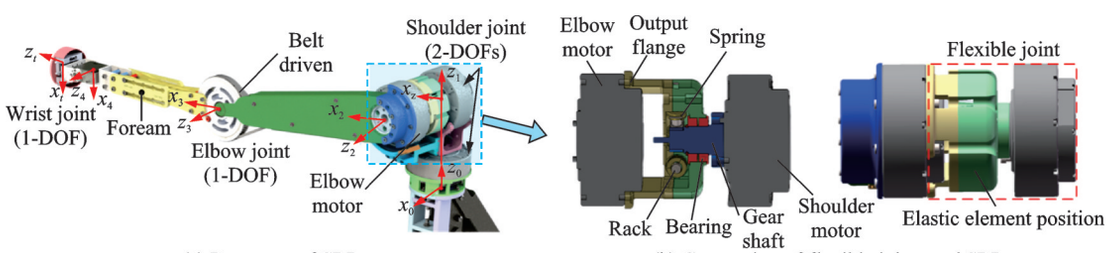

(a) Prototype of SRLs (b) Connection of flexible joints and SRLs

Fig.1 Structure of SRLs

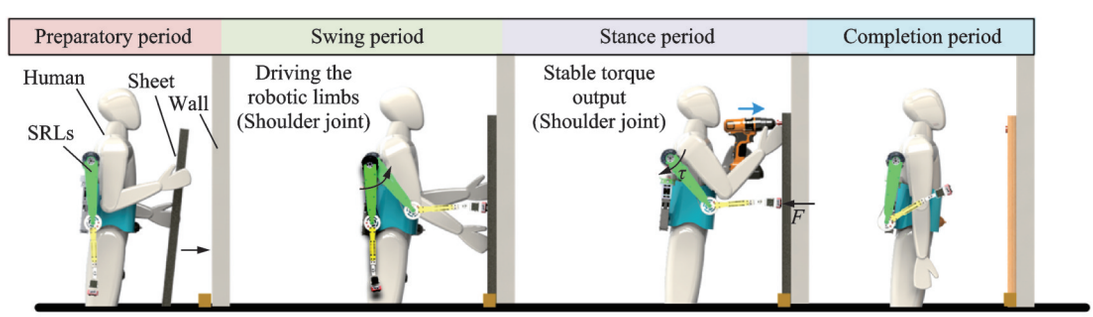

Fig.2 Workflow of SRLs to assist in sheet installation

1.2 Human-robot safety design indicators

This paper proposes design indicators for the flexible joints of SRLs based on the passive safety requirements during sheet support. In the investigation of human-robot collision safety and the peak force impacting human body injury, certain scholars have established a safety threshold of 50 N for external force[23]. Through the analysis of peak collision forces and the corresponding formula of joint stiffness K, along with the physical parameters of the SRLs, it can be inferred that joint stiffness should satisfy $K \leqslant 64.66$ N·m/rad. Furthermore, by analyzing the model of operation in the work plane, the required maximum output torque of the shoulder joint is 2.07 N·m. Simultaneously, the design of the joints should adhere to the principles of lightweighting. The design indicators are summarized in Table 1.

Table 1 Design indicators

Design indicator	Value
Stiffness/(N•m•rad^{-1})	≤64.66
Output torque/(N•m)	≥2.07
Mass/g	≤250 (Without motor)

2 Structure Design and Analysis of SEJ with Segmental Stiffness

The structure of SEJ is shown in Fig.3. In this illustration, the rack's center is positioned at a distance R from the geometric center of the output flange. The spring radius is r, the stiffness is k, and the total length of the spring set is H.

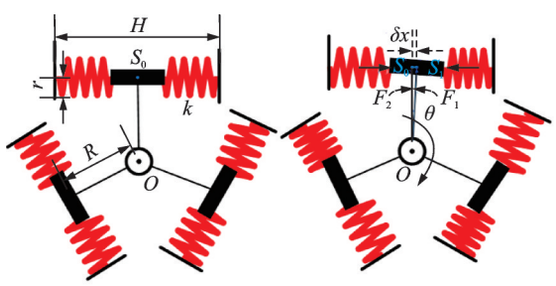

Fig.3 Design principles of elastic units for SEJ

When the elastic unit is deflected by an angle θ, the geometric center S_0 of the spring assembly is displaced from its initial position by δx. Under this condition, there are two possible states of the compression springs: (1) All the springs are in compression, and (2) one spring is in compression, and the other one returns to the free state.

When the mechanism deflection angle is less than θ_0 ($\theta \leqslant \theta_0$), springs on both sides of the rack are compressed. Within this range, the displacement δx of the rack, and the torque τ applied to springs are defined as

$$F_1 = k(x_0 + \delta x) \tag{1}$$

$$F_2 = k(x_0 - \delta x) \tag{2}$$

$$\delta x = R\tan\theta \tag{3}$$

$$\tau = (F_1 - F_2)R = 2kR^2\tan\theta \tag{4}$$

where x_0 is the pretension length of spring.

Due to the spring radius, the proximal and distal ends of the output flange's geometric center experiences different torques. According to the mean value theorems for definite integrals and Eq.(4), the torque of a set of springs can be obtained.

$$\tau_1 = \frac{1}{2-r}\int_{R-r}^{R+r} 2kx^2\tan\theta\,\mathrm{d}x = 2k\tan\theta\left(R^2 + \frac{r^2}{3}\right) \tag{5}$$

Assuming that three sets of springs are arranged in an equilateral triangle configuration, the resulting combined torque and joint stiffness can be derived as

$$\tau_{\text{total}} = 3\tau_1 = 6k\tan\theta\left(R^2 + \frac{r^2}{3}\right) \tag{6}$$

$$K = \frac{\mathrm{d}\tau_{\text{total}}}{\mathrm{d}\theta} = 6k\left(R^2 + \frac{r^2}{3}\right)(1 + \tan^2\theta) \tag{7}$$

When $\theta \geqslant \theta_0$, only one of the springs is under compression, while the other one returns to the free state. Consequently, the resulting combined torque and joint stiffness are obtained as

$$\tau_{\text{total}\,2} = 3k\tan\theta\left(R^2 + \frac{r^2}{3}\right) + 3k\tan\theta_0\left(R^2 + \frac{r^2}{3}\right) \tag{8}$$

$$K = \frac{\mathrm{d}\tau_{\text{total}\,2}}{\mathrm{d}\theta} = 3k\left(R^2 + \frac{r^2}{3}\right)(1 + \tan^2\theta) \tag{9}$$

From the above analysis, it can be seen that the joint stiffness reduces to half of its normal operating range when $\theta \geqslant \theta_0$, enhancing its ability to buffer collision.

2.1 Functional design of SEJ with segmental stiffness characteristic

To achieve the segmented stiffness characteristic in the SEJ, x_0 is adjusted to create two distinct stiffness curves. This design aims to maintain high stiffness when the mechanism deflection angle is small and maintain lower sitffness when the mechanism deflection exceeding the safety threshold. The safety threshold angle is established based on the Eq.(10).

$$\theta_0 = \arctan\left(\frac{x_0}{R}\right) \tag{10}$$

The design of SEJ is constrained by the size limitation. The primary objective is to ensure that the maximum output torque exceeds 2.07 N·m. Slight perturbations from human movement can lead to increases in load torque. To enhance safety and accommodate such variations in torque, a maximum safety torque of 2.6 N·m is established. Through the utilization of Eq.(8), the safety threshold angle is calculated to be 5.5°. Employing Eq.(10), the pretension length of the spring is determined. The segmental stiffness principle is shown in Fig.4.

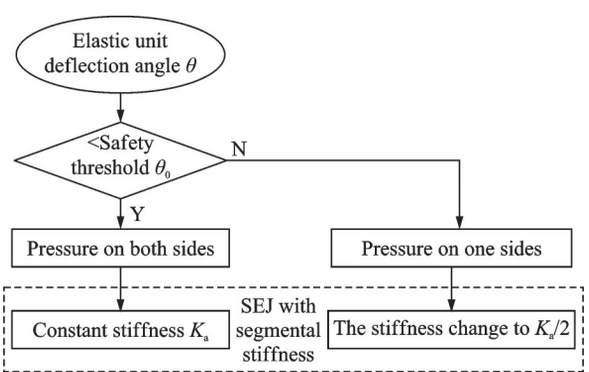

Fig.4 Segmental stiffness principle of SEJ

The SEJ is illustrated in Fig.5. It is engineered to convert motor rotation into linear spring deformation, which is then transmitted to the joint output. The SEJ comprises three compression springs arranged in an equilateral triangle configuration. During operation, when the motor rotates, it drives the gear shaft to rotate. As the gear shaft rotates, it compresses the springs. The compressed springs then transfer this mechanical energy to the output flange, achieving flexible transmission and reducing the impact.

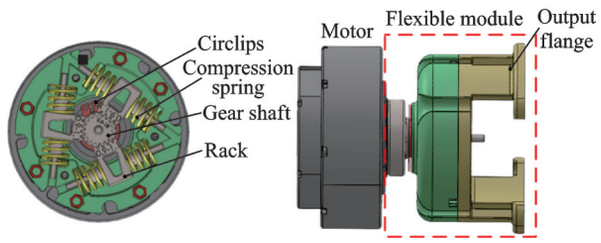

Fig.5 SEJ prototype

2.2 Transmission parameter optimization for SEJ

To evaluate the effect of different transmission parameters in practical applications, this paper outlines four distinct configurations, as detailed in Table 2. The optimal configuration will be selected.

Table 2 Configuration parameters of SEJ

Parameter name	Configuration groups			
	Ⅰ	Ⅱ	Ⅲ	Ⅳ
Gear shaft m_t/mm	0.9	0.9	1.375	0.5
Gear shaft z_t	18	18	12	36
Rack m_t/mm	0.9	0.9	1.375	0.5
Rack z_t	4	5	3	8
Rack length L/mm	11.9	16.0	16.0	16.0
Spring pretension length x_a/mm	0	2.04	2.04	2.04

Due to variations in gearing parameters, it is essential to first evaluate the strength of different configurations. Configurations that meet the strength requirements will be selected. Subsequently, real stiffness identification experiments are conducted based on the experimental setup shown in Fig.6. The configuration with the smallest error is selected as the optimal.

In this paper, 3D printing is used to process non-standard parts, and the material is nylon material. The rack and shaft of the four configurations will be calibrated for strength. The root bending fatigue strength is calculated as

$$\sigma_F = \frac{2KT_1Y_{FS}}{\varphi_d m^3 z^2} \tag{11}$$

where σ_F is the root bending fatigue strength. K is the load factor, $K = K_A K_V K_\beta K_\alpha$, where K_A is the application factor, K_V the dynamic factor, K_β the load distribution factor, and K_α the load sharing fac-

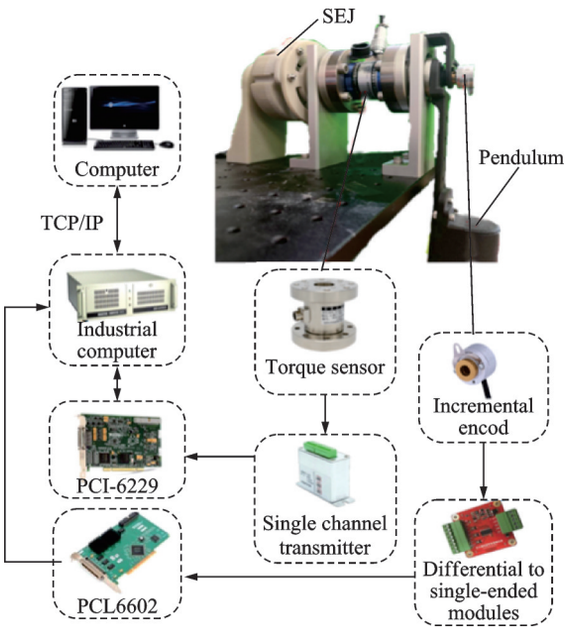

Fig.6 Stiffness identification experiment setup

tor. Y_{FS} is the combined tooth form factor, $Y_{FS}=Y_{Sa}Y_{Fa}$, where Y_{Sa} is the stress correction factor, and Y_{Fa} the tooth form factor. T_1 is the torque, φ_d the face width factor, m the module, and z the number of teeth.

The surface contact fatigue strength is calculated as

$$\sigma_H=\sqrt{\frac{2KT_1}{\varphi_d d^3}\frac{u+1}{u}}Z_H Z_E \tag{12}$$

where σ_H is the surface contact fatigue strength, Z_H the zone factor, and Z_E the elasticity factor. u is the transmission ratio, which is taken to be infinity here. d is the pitch diameter of the gear.

Following the Eq.(11), the root bending fatigue strength of configuration Ⅳ is 56 MPa, which exceeds the specified limit 44 MPa. The configuration Ⅳ does not meet the requirement and is therefore discarded.

Eventually, the SEJ under configurations Ⅰ, Ⅱ, and Ⅲ are manufactured, and its prototype structure is shown in Fig.7. The mass of the SEJ is 233 g (without motor), which can meet lightweight design indicators.

To verify the stiffness characteristics of the SEJ, an experimental device as shown in Fig.6 is designed for static stiffness tests. In the experiment, the input shaft of the SEJ is fixed. The torque is exerted on the output shaft of the SEJ by the deflection of the pendulum. Torque sensors (DYLN-101, Rated output: 1.0—2.0 mV/V) record torque, encoders (K22, Resolution: 1 600 P/R) record angles. The results are shown in Fig.8.

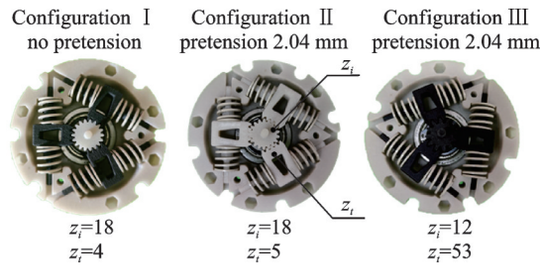

Fig.7 SEJ prototype of different configurations

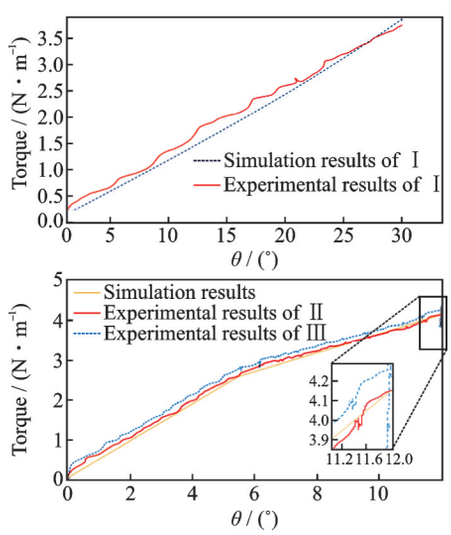

Fig.8 Stiffness of SEJ with different configurations

To quantitatively evaluate the effectiveness of our optimization, the error is defined as

$$\text{error}=\frac{\max|\tau_{\text{simulation}}-\tau_{\text{real}}|}{\tau_{\max,\text{simulation}}}\times 100\% \tag{13}$$

where $\tau_{\text{simulation}}$ is the simulated stiffness, τ_{real} the real stiffness, and $\tau_{\max,\text{simulation}}$ the maximum stiffness of simulation.

It can be seen that the errors of Ⅰ, Ⅱ and Ⅲ are 7.9%, 5.1% and 6.8% respectively. The curve of Ⅰ is not segmented, because the spring is always free on one side if it is not preloaded. This spring is easy to shift its position during operation, which affects the reliability of the transmission. In configuration Ⅲ, a torque recession occurs at the end because of the large modulus of the Ⅲ, resulting in a small number of teeth. After rotating to a certain an-

gle, the phenomenon of single tooth meshing or toothless meshing will occur. It will greatly affect the reliability of the transmission system. Finally, configuration Ⅱ is selected as the optimal configuration.

3 Buffer Performance Evaluation of SEJ, PVSJ and RJ in Dynamic Collisions

To evaluate the dynamic collision buffering performance of the SEJ and demonstrate the performance difference of SEJ, PVSJ and RJ, this paper conducts dynamic collision experiments. The PVSJ and RJ are shown in the Fig.9.

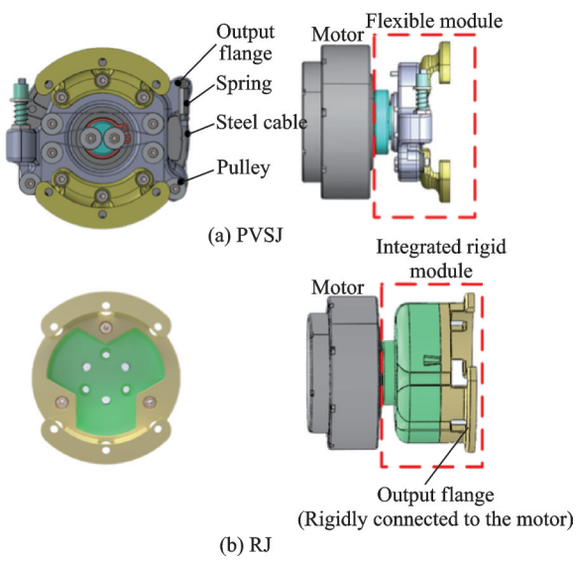

Fig.9 RJ and PVSJ prototypes

The PVSJ has flexible module inside. It achieves variable stiffness through a special four-link mechanism, and its stiffness is shown as[24]

$$K=\frac{\partial\tau}{\partial\theta}=N^2\left(s^2L^2+s^2\frac{\partial L}{\partial\theta}\delta l_2+s\frac{\partial s}{\partial\theta}L\delta l_2\right)k+Ns\frac{\partial L}{\partial\theta}F_0 \tag{14}$$

where F_0 is the spring pretension, k the stiffness of spring, N the working branch, and other parameters are related to its geometric shape. In past studies[25] which are shown in Fig.10, the optimal parameters of this PVSJ have been established. The spring stiffness is 6 N/mm, the pretension is 20 N and the working branch is 2.

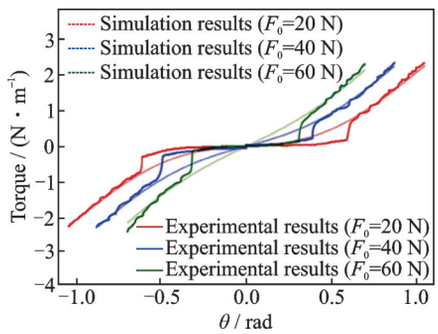

Fig.10 Torque-deflection curves for PVSJ with different parameters[25]

The RJ has no elastic elements inside, and it is driven directly by the motor. The integrated rigid module is 3D printed from nylon material.

The SEJ configuration and parameters are consistent with the configuration II in Section 2.

3.1 Experiment of torque measurement in dynamic collision

The experimental setup for dynamic collision torque measurement is depicted in Fig.11. The SRLs are installed to the base and the initial position of robotic limbs is vertical to the ground. The obstacle for collision is positioned 40 cm in front of robotic limbs. The collision position is the forearm of SRLs, which is about 50 cm away from shoulder joints. After the collision of about 3 s, the motor reverses and returns to its initial position. Shoulder joints are driven by DC motors (HT-04, Nominal torque: 13 N·m), and the driven-speed are 3 (°)/s, 5 (°)/s and 7 (°)/s. Each of the three joints is installed on the shoulder of SRLs, and collision experiments are conducted. The feedback torque of the motor during the collision is measured.

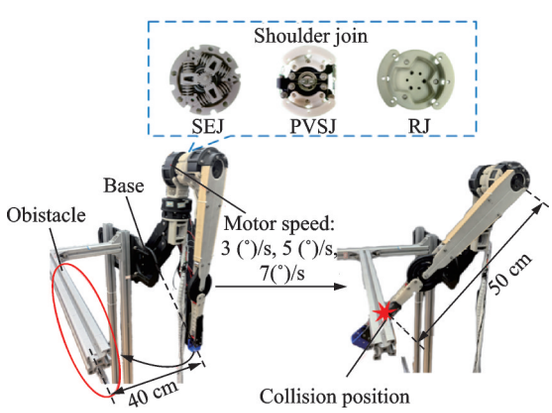

Fig.11 Experimental setup for torque measurement

To demonstrate the buffering effect of flexible joints more clearly, this paper compares the torque by different joints during the dynamic collisions. The result is shown in Fig.12.

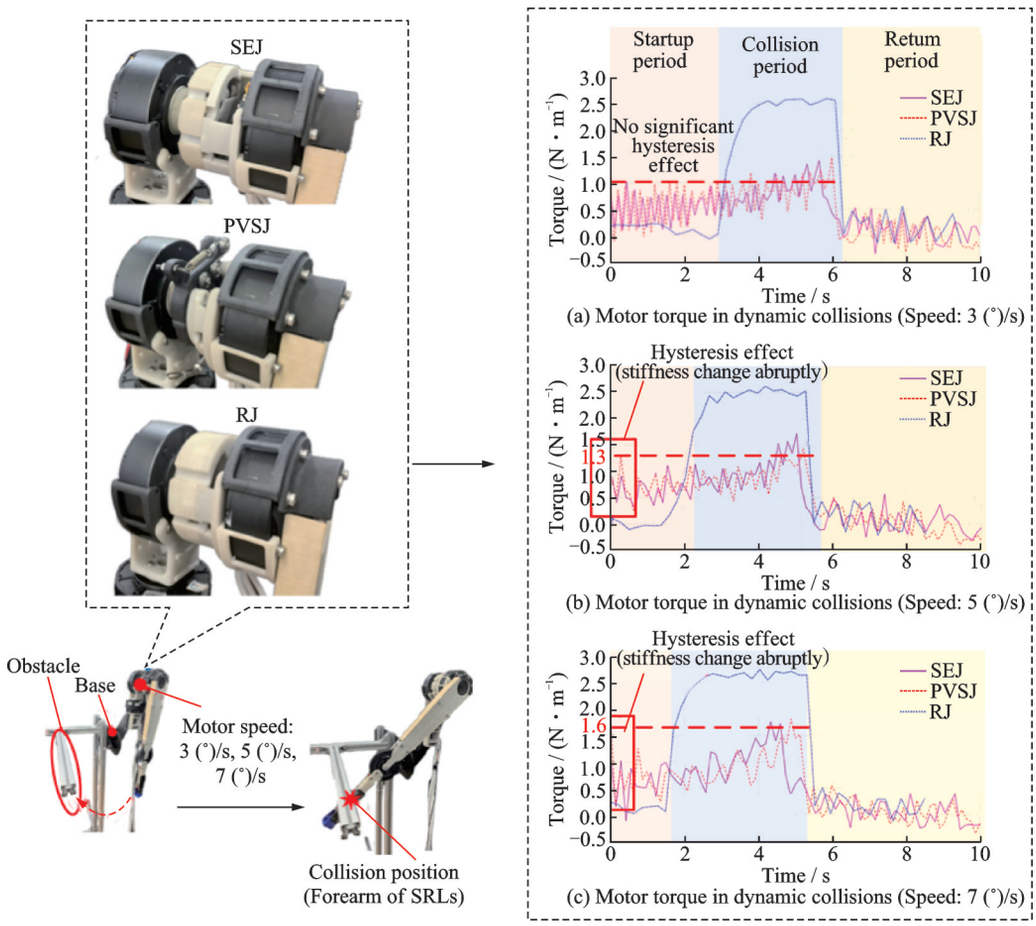

Fig.12 Results of dynamic collision torque measurement

According to Fig.12, it can be seen that when the motor speed is 3 (°)/s, the torque of the RJ increases by about 2 200 % during the collision. The measured value is approximately 22 times that of the startup period, which poses a potential risk to the robot's shoulder joint. In contrast, both SEJ and PVSJ demonstrate good buffering performance. The torque of SEJ and PVSJ only increase by 190% and 183%, respectively. And most of the impacts are absorbed by the flexible joints. When the motor speed is 5 (°)/s, the torque of RJ increases by about 2 500% during the collision, while torques of the SEJ and PVSJ increase by about 190% and 170%, respectively. When the motor speed is 7 (°)/s, torques of RJ, SEJ and PVSJ increase by about 1 600%, 175% and 180%, respectively. The results show that the flexible joint can effectively buffer the shock of the motor during dynamic collision.

In addition, when the motor speeds are 5 (°)/s and 7 (°)/s, the torque of the PVSJ increases suddenly during the startup period due to the hysteresis effect. The increased torque is similar to the peak of collision. It means that the motor with PVSJ is subjected to a torque increase suddenly with every startup. It is unstable and unsafe for the normal operation of the robot.

At a motor speed of 3 (°)/s, the hysteresis effect is negligible. In contrast, at speeds of 5 (°)/s and 7 (°)/s, the hysteresis effect becomes more pronounced. This phenomenon may be attributed to the fact that at higher motor speeds, the tendon undergoes rapid deformation, but its response lags behind the actuation, worsening the hysteresis effect. Con-

versely, at slower motor speeds, the tendon has more time to response, and the dynamic effects of friction and material deformation may be decreased, leading to a less noticeable hysteresis effect.

To evaluate the dynamic collision buffer performance of different joints quantitatively, the parameter buffer performance (BP) is utilized. The formula for the BP_{torque} is shown as

$$BP_{torque} = \frac{\tau_{max,RJ} - \tau_{max,FJ}}{\tau_{max,RJ}} \times 100\% \quad (15)$$

where $\tau_{max,RJ}$ is the max collision torque of RJ and $\tau_{max,FJ}$ the max collision torque of flexible joint. The higher the value of BP_{torque}, the better effect of buffering torque. The specific values of each joint are organized in Table 3.

Table 3 BP_{torque} of SEJ and PVSJ

Motor speed/ ((°)•s^{-1})	Max collision torque/(N•m)			BP_{torque}/%	
	RJ	SEJ	PVSJ	SEJ	PVSJ
3	2.606 6	1.428 6	1.481 3	45.2	43.2
5	2.624 2	1.727 5	1.454 9	34.2	44.6
7	2.756	1.762 6	1.815 4	36.0	34.1

According to Table 3, it can be seen that when the speed is 3 (°)/s, the BP_{torque} of SEJ and PVSJ are respectively 45.2% and 43.2%. The BP_{torque} of SEJ decreases to 34.2% when the motor speed is 5 (°)/s. This is because the metal springs in SEJ may display non-linear stiffness at high speeds, resulting in incomplete energy absorption. When the motor speed is 7 (°)/s, the BP_{torque} of SEJ and PVSJ respectively decrease to 36% and 34.1%. Higher speed collisions are more impactful and generate more collision energy, reducing the buffering effect of flexible joints. Notably, it can be seen that the BP_{torque} of SEJ is 34.2%—45.2%, the BP_{torque} of PVSJ is 34.1%—44.6%, which is similar and demonstrates the effectiveness of flexible joints in collision buffering. And their buffering capacity is similar.

In summary, due to the PVSJ's inherent hysteresis effect in startup period, the robot's operation is unstable. Meanwhile, the SEJ buffers 34%—45% collision torque, and the torque does not change suddenly in the startup period. It demonstrates that the SEJ performs more stable in terms of human-robot safety.

3.2 Experiment of force measurement in dynamic collision

The experimental setup for dynamic collision force measurement is depicted in Fig.13.

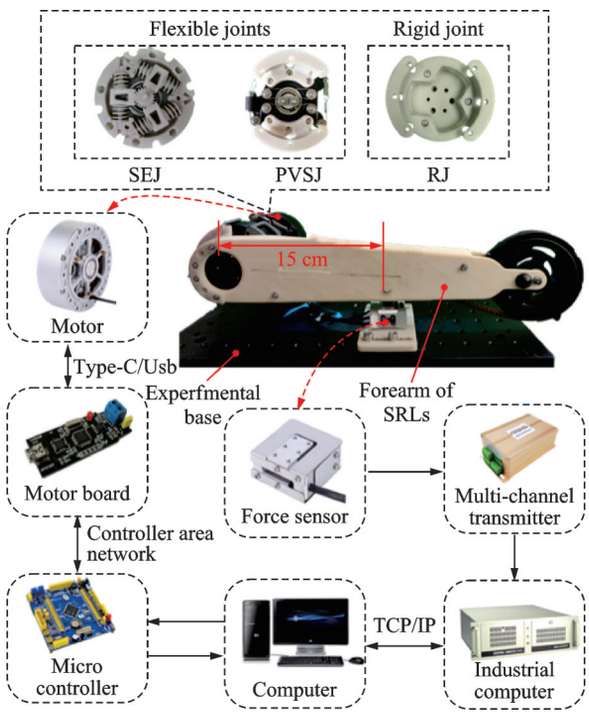

Fig.13 Experimental setup for force measurement in dynamic collision

In the dynamic collision experiment, the initial position of the SRLs upper arm is precisely controlled at 5.5° from the horizontal position. The drive motor rotates both the RJ the flexible joints with driven-torques of 1, 2, 3 and 4 N·m, respectively. The robotic arm then collides with force sensors(FNZ-50 N, Resolution: 0.1 N)to measure dynamic collision forces. Before each experiment, the force sensors are calibrated using standard weights. The results are presented in Fig.14.

To evaluate the dynamic collision buffer performance quantitatively, the BP_{force} is utilized. The formula for the BP_{force} is shown as

$$BP_{force} = \frac{F_{max,RJ} - F_{max,FJ}}{F_{max,RJ}} \times 100\% \quad (16)$$

where $F_{max,RJ}$ is the max collision force of RJ. The higher the value of BP_{force}, the better the buffering effect. The BP_{force} of each parameter are organized in Table 4.

According to Table 4, when the driving torque is 1 N·m, the BP_{force} of SEJ and PVSJ are 58.7%

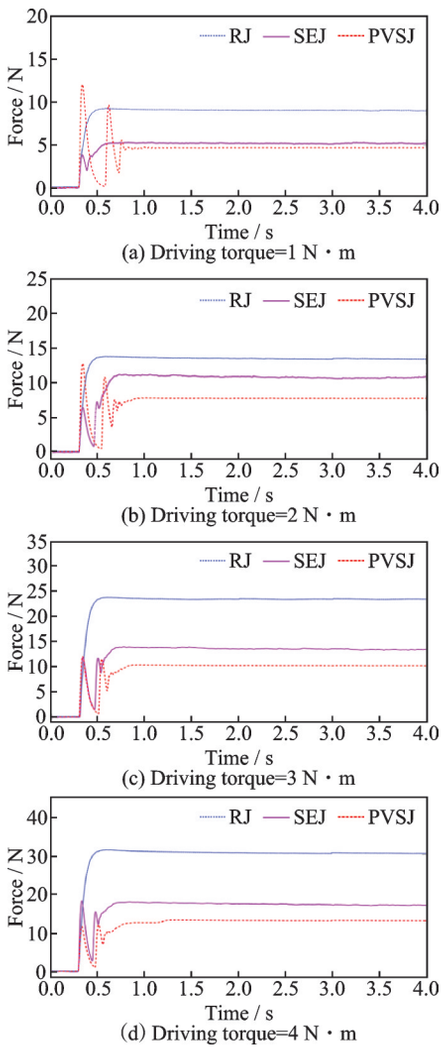

Fig.14 Results of dynamic collision force measurement

Table 4 BP_{force} of SEJ and PVSJ

Torque/ (N•m)	Max collision force/N			BP_{force}/%	
	RJ	PVSJ	SEJ	PVSJ	SEJ
1	9.2	12.1	3.8	−31.5	58.7
2	13.5	12.8	6.3	5.18	53.3
3	23.8	12.2	12.2	48.7	48.7
4	30.7	11.6	18.2	62.2	40.7

and −31.5%, respectively. It means the maximum collision force of PVSJ is even greater than RJ. This negative buffering effect is attributed to the hysteresis effect inherent in the PVSJ during the loading phase at lower torques. Specifically, when overcoming static friction, the PVSJ deflects at a larger angle and accumulates more elastic potential energy, resulting in the maximum instantaneous collision force which exceeds that of RJ. When the driving torque is 2 N·m, the BP_{force} of SEJ and PVSJ are 53.3% and 5.18%, respectively. The BP_{force} of PVSJ is only 5.18%, which is insufficient to ensure the safety of both human and robot. When the driving torque is 3 N·m, both the BP_{force} of SEJ and PVSJ are 48.7%. It demonstrates the two flexible joints are comparable in buffering collisions. When the driving torque is 4 N·m, the BP_{force} of SEJ and PVSJ are 62.2% and 40.07%, respectively. It demonstrates both PVSJ and SEJ can buffer the collisions well and the PVSJ has better performance than SEJ.

In a word, in dynamic collisions, the collision force buffering performance of PVSJ is unstable. The PVSJ creates a negative effect when the driving torque is 1 N·m, and the collision force buffering performance is only 5% when the driving torque is 2 N·m. In contrast, the SEJ has more stable collision force buffering performance in dynamic collisions. The SEJ is able to buffer 40.7%—58.7% collision force.

3.3 Results

Through above dynamic collision experiments, the buffering performance of different joints is quantitatively evaluated. Experimental results indicates that both the SEJ and PVSJ are capable of buffering impac in dynamic collisions. However, when the motor speed exceeds 5 (°)/s, the joint torque with PVSJ undergoes an increase abruptly which is almost equivalent to a collision. This phenomenon is attributed to the inherent hysteresis effect of PVSJ. In addition, when the driven torque is 1 N·m, the BP_{force} of PVSJ is negative, indicating that the PVSJ increases the collision force compared to the RJ. The two phenomena describe above may compromise the safety and stability of the robot during normal operation.

In contrast, the SEJ demonstrates greater stability during dynamic collisions. Because it can buffer 40.7%—58.7% of collision force and 34.2%—45.2% of collision torque, and there are no negative effects. The SEJ enables SRLs to operate more safely in human-robot collaboration.

In a word, compared to the PVSJ, the SEJ is more stable at different speeds and torque-driven in dynamic collisions.

4 Discussion

4.1 Exploring the hysteresis effect of PVSJ

Because of the PVSJ's design and principle, hysteresis effects are inherently[25]. To further explore the cause of the hysteresis effect of the PVSJ, the stiffness of the PVSJ is tested based on the platform shown in Fig.6. The experimental results are shown in Fig.15. Meanwhile, the stiffness error of the PVSJ is evaluated based on Eq.(13).

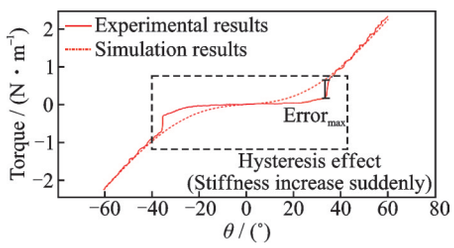

Fig.15 Real stiffness of PVSJ

According to Fig.15, it can be seen that the error of PVSJ is 23.04%, which is mainly caused by the hysteresis effect. This is because when the mechanism is deflected, the friction and the tension of the tendon are not uniformly distributed. When the deflection angle of the mechanism is small, the PVSJ cannot overcome the friction, resulting in a gradual increase of the joint torque. During this period, the actual stiffness is much lower than the theoretical stiffness. When the deflection angle exceeds a certain threshold, the PVSJ can overcome the friction and the rope quickly returns to the normal level. During this period, the actual stiffness increases abruptly, thereby exacerbating the instability of the PVSJ.

Hysteresis effects have the potential to influence the stability of wearable robotic systems. For example, when the robot is subjected to external impacts, delays in joint torque response may increase the risk of injury to the wearer.

4.2 Significance and limitations of the work

In this paper, a SEJ with segmental stiffness is developed and evaluated. The above experimental results reflect that the application of SEJ greatly increases the safety of both humans and robots. Furthermore, under certain motor parameters, robots equipped with flexible joints execute smooth movements, whereas robots with rigid joints tend to exhibit chatter. This is because the flexible elements can absorb and release energy, which avoids chatter.

In addition, to more effectively assess the human-robot safety performance of SEJ, a systematic comparison of the three joint types is conducted. Based on the above experiments, it is demonstrated that the SEJ exhibits more stable and reliable human-robot safety performance compared to the PVSJ.

There are some limitations in this paper. For example, the collision buffering performance of the flexible joints is not evaluated at higher speeds. Because the material strength is insufficient to support higher-speed dynamic collision experiments. Besides, it is observed that the flexible joints increase the difficulty of position control. Because the motor first compresses the elastic element. After reaching a specific level of compression, the flexible joint actuates the robotic limb. During this process, the relationship between the motor deflection and the deflection of the robotic limb is inherently nonlinear. Consequently, the researchers use external sensors such as encoders to solve this problem. With the introduction of encoders, the position control becomes more complicated.

5 Conclusions

To improve the collaboration safety between the wearer and SRLs, this paper designs a SEJ with segmental stiffness mounted on the shoulder of SRLs. In addition, this paper compares the human-robot safety buffer performance of SEJ and PVSJ under different conditions. The results indicate that the SEJ is capable of absorbing 40.7%—58.7% of the collision force and 34.2%—45.2% of the collision torque under dynamic collision conditions. Moreover, compared to the PVSJ, which exhibits a stiffness error of 23.04%, the SEJ demonstrates a significantly lower stiffness error of 5.1%. As a result, the SEJ demonstrates greater stability and is more suitable for application in SRLs.

In the future work, both the PVSJ and SEJ will be further optimized to enhance the performance of human-robot safety. This includes reducing hysteresis effects in the PVSJ and employing high-strength materials.

References

[1] LIAO Z Y, CHEN B, CHANG T Z, et al. A human augmentation device design review: Supernumerary robotic limbs[J]. Industrial Robot: the International Journal of Robotics Research and Application, 2023, 50(2): 256-274.

[2] LIU Keming, CHEN Bai, XU Jiajun, et al. Structural design and compensation control of supernumerary robotic limbs for overhead work[J]. Transactions of Nanjing University of Aeronautics and Astronautics, 2023, 40(6): 727-737.

[3] DOMINIJANNI G, SHOKUR S, SALVIETTI G, et al. The neural resource allocation problem when enhancing human bodies with extra robotic limbs[J]. Nature Machine Intelligence, 2021, 3(10): 850-860.

[4] LIU Debin, WANG Dan, CHEN Bai, et al. A survey of supernumerary robotic limbs[J]. Journal of Zhejiang University (Engineering Science), 2021, 55(2): 251-258.(in Chinese)

[5] NANDESHWAR N, HUMPHRIES J, AMER N. Optimization of the speed & separation monitoring protective separation distance in human-robot collaboration safety systems[C]//Proceedings of the 2022 7th International Conference on Mechanical Engineering and Robotics Research (ICMERR). Krakow, Poland: IEEE, 2022: 157-162.

[6] HERBSTER S, BEHRENS R, ELKMANN N. Modeling the contact force in constrained human-robot collisions[J]. Machines, 2023, 11(10): 955.

[7] HARDER M, ISKANDAR M, LEE J, et al. Extensions to dynamically-consistent collision reaction control for collaborative robots[C]//Proceedings of the 2023 IEEE/RSJ International Conference on Intelligent Robots and Systems (IROS). Detroit, USA: IEEE, 2023: 5982-5988.

[8] LIU Qian, LIU Chuankai, ZHU An, et al. Ground simulation and verification method for motion control of space manipulator[J]. Journal of Nanjing University of Aeronautics & Astronautics, 2022, 54(1): 58-67.(in Chinese)

[9] HASANEN B B, AWAD M I, BOUSHAKI M N, et al. Novel supernumerary robotic limb based on variable stiffness actuators for hemiplegic patients assistance[C]//Proceedings of the 2022 IEEE/RSJ International Conference on Intelligent Robots and Systems (IROS), Kyoto, Japan: IEEE, 2022: 1892-1899.

[10] FERN' ANDEZ J, SPRENGEL H, MALLWITZ M, et al. Designing modular series-elastic actuators for safe human-robot collaboration in industrial settings[M]//Advances in Cooperative Robotics. [S.l.]: World Scientific, 2016: 135-142.

[11] AWAD M I, HUSSAIN I, GAN D M, et al. Passive discrete variable stiffness joint (pDVSJ-Ⅱ): Modeling, design, characterization, and testing toward passive haptic interface[J]. Journal of Mechanisms and Robotics, 2019, 11(1): 011005.

[12] ZHANG T, HUANG H. Design and control of a series elastic actuator with clutch for hip exoskeleton for precise assistive magnitude and timing control and improved mechanical safety[J]. IEEE/ASME Transactions on Mechatronics, 2019, 24(5): 2215-2226.

[13] TSAGARAKIS N G, LAFFRANCHI M, VANDERBORGHT B, et al. A compact soft actuator unit for small scale human friendly robots[C]//Proceedings of the 2009 IEEE International Conference on Robotics and Automation. Kobe, Japan: IEEE, 2009: 4356-4362.

[14] HAM R V, SUGAR T G, VANDERBORGHT B, et al. Compliant actuator designs[J]. IEEE Robotics & Automation Magazine, 2009, 16(3): 81-94.

[15] LIU Y W, WANG D Q, YANG S K, et al. Design and experimental study of a passive power-source-free stiffness-self-adjustable mechanism[J]. Frontiers of Mechanical Engineering, 2020, 16(1): 32-45.

[16] TOUBAR H, AWAD M I, BOUSHAKI M N, et al. Design, modeling, and control of a series elastic actuator with discretely adjustable stiffness(SEADAS)[J]. Mechatronics, 2022, 86: 102863.

[17] QIAN Y P, HAN S S, AGUIRRE-OLLINGER G, et al. Design, modeling, and control of a reconfigurable rotary series elastic actuator with nonlinear stiffness for assistive robots[J]. Mechatronics, 2022, 86: 102872.

[18] CHEN Y L, HUANG Y J, CHEN K B, et al. Novel torsional spring with corrugated flexible units for series elastic actuators for cooperative robots[J]. Journal of Mechanical Science and Technology, 2022, 36(6): 3131-3142.

[19] WANG P C, ZHU Q G, HU X H, et al. Research on interaction safety of human-robot collision based on series elastic actuator[C]//Proceedings of the 2018 5th International Conference on Information, Cybernetics, and Computational Social Systems (ICCSS). Hangzhou, China: IEEE, 2018: 180-185.

[20] WOLF S, HIRZINGER G. A new variable stiffness design[C]//Proceedings of the 2008 IEEE International Conference on Robotics and Automation. Pasadena, USA: [s.n.], 2008: 1741-1746.
[21] CALANCA A, DIMO E, VICARIO R, et al. Introducing series elastic links for affordable torque-controlled robots[J]. IEEE Robotics and Automation Letters, 2019, 4(1): 137-144.
[22] PARK J J, SONG J B. Safe joint mechanism using inclined link with springs for collision safety and positioning accuracy of a robot arm[C]//Proceedings of the 2010 IEEE International Conference on Robotics and Automation. Anchorage, USA: IEEE, 2010: 813-818.
[23] YAMADA Y, HIRASAWA Y, HUANG S, et al. Human-robot contact in the safeguarding space[J]. IEEE/ASME Transactions on Mechatronics, 1997, 2(4): 230-236.
[24] LI Z Y, BAI S P, MADSEN O, et al. Design, modeling and testing of a compact variable stiffness mechanism for exoskeletons[J]. Mechanism and Machine Theory, 2020, 151: 103905.
[25] LIU K M, CHEN B, LIAO Z Y, et al. Structural design and stiffness characteristics of a passive variable stiffness joint[C]//Proceedings of the 2023 Intelligent Robotics and Applications (ICIRA). Singapore: Springer Nature Singapore, 2023: 398-409.

Acknowledgements This work was supported by the National Natural Science Foundation of China (No. U22A20204) and the Innovation Foundation from National Clinical Research Center for Orthopedics, Sports Medicine & Rehabilitation Foundation (No. 23-NCRC-CXJJ-ZD3-8).

Authors

The first author Mr. **XIAO Yao** received the B.S. degree in mechanical engineering from Soochow University, Suzhou, China, in 2023. He is now a M.S. student in Nanjing University of Aeronautics and Astronautics, Nanjing, China. His research interest is wearable robot.

The corresponding author Prof. **CHEN Bai** received the Ph.D. degree at Zhejiang University in 2005. Now he is a professor at College of Mechanical and Electrical Engineering, Nanjing University of Aeronautics and Astronautics. His current research interests include minimally invasive neurosurgery robot, virtual surgery system, force feedback control, wearable robot.

Author contributions Mr. **XIAO Yao** designed the study and wrote the manuscript. Dr. **LIAO Ziyu** optimized the overall idea. Mr. **QU Wenjie** conducted resource collection. Dr. **CHANG Tianzuo** interpreted the results. Mr. **LIU Keming** contributed to data and helped the experiments. Prof. **CHEN Bai** guided on the research and contributed to the funding acquisition. All authors commented on the manuscript draft and apprved the submission.

Competing interests The authors declare no competing interests.

(Production Editors: XU Chengting, WANG Jie)

一种用于外肢体机器人人机安全的串联弹性关节的开发和实验评估

肖 遥[1], 廖梓宇[1,2], 渠文杰[1], 常天佐[1], 刘珂铭[1], 陈 柏[1]

(1.南京航空航天大学机电学院,南京 210016,中国; 2.金华职业技术大学智能制造学院,金华 321017,中国)

摘要:人机安全是穿戴式机器人领域的热点问题,在外肢体机器人(Supernumerary robotic limbs, SRLs)的研究中尤为突出。柔性关节的提出使得人和机器人可以柔顺接触,而非严格约束彼此的运动,这一技术显著优化了人机安全策略。然而,现有研究主要集中于柔性关节的变刚度特性分析,而对其在人机碰撞场景下的动态性能评估则相对匮乏。因此,本文通过动态碰撞实验,对串联弹性关节(Series elastic joint,SEJ)和被动变刚度关节(Passive variable stiffness joint,PVSJ)的缓冲人机碰撞性能进行了比较分析。结果表明,相较于刚性关节,SEJ在特定条件下(驱动力矩不大于4 N•m或驱动速度3~7 (°)/s)可缓冲40.7%~58.7%的碰撞力和34.2%~45.2%的碰撞力矩,并且其性能稳定性显著优于PVSJ。同时,SEJ的刚度误差为5.1%,显著低于PVSJ的23.04%,PVSJ较大的刚度误差直接导致其在碰撞缓冲过程中不稳定。基于上述分析证实,SEJ在动态碰撞缓冲中具有更稳定的人机安全性能,更适合应用于外肢体机器人的人机安全防护场景。

关键词:外肢体机器人;变刚度关节;串联弹性关节;人机安全;穿戴式机器人